SUPPORTING INFORMATION

SUPPORTING EXPERIMENTAL PROCEDURES

Antibody. For the production of mAbs to rabbit MG23, two synthetic peptides corresponding to residues 34-50 at the N-terminus and 217-235 at the C-terminus were conjugated with keyhole limpet hemocyanin and then repeatedly injected into BALB/c mice. Hybridoma cells expressing mAbs were generated using splenocytes from the immunized mice (*11*). Immunohistochemical and immunoblot experiments established that clones mAb7 (mAb-N) and mAb251 (mAb-C) specifically recognize their antigenic epitopes.

Topology analysis. SR vesicles were prepared from rabbit skeletal muscle (*13*). Rabbit MG23 cDNA was subcloned into pcDNA3.1 (Invitrogen), and the FLAG tag sequence (Sigma) was introduced into the protein-coding region at several sites. The resulting plasmids were transfected using lipofectoamine according to the instruction manual (Invitrogen), and ER vesicles were prepared from HEK293 cells under isotonic conditions (*14*). The transmembrane topology of MG23 was examined as essentially described previously (*14, 15*). The SR/ER vesicles were suspended in the buffer containing 10 mM Hepes-KOH (pH 7.4), 100 mM NaCl, 10 mM KCl, 1.5 mM $MgCl_2$, 5 mM EDTA, 5 mM EGTA and 0.25 M sucrose, and treated with varying concentrations of proteinase K in the absence or presence of 0.1% SDS. The reactions were stopped by adding phenylmethylsulfonyl fluoride and the protein degradability was analyzed by immunoblotting using mAb-N, mAb-C and mAb to FLAG-tag sequence (Sigma-Aldrich).

Purification of native MG23. Total SR membrane was prepared from rabbit skeletal muscle (*13*), and SR proteins were solubilized in a buffer containing 1% NP-40, 0.25 M sucrose, 2 mM melcaptoethanol, 0.3 M NaCl, 50 mM Tris-HCl or 10 mM Hepes (pH 7.4) and protease inhibitors at ~6 mg/ml protein for 45 min. After diluting the detergent content to 0.5%, insoluble materials were removed by ultracentrifugation, and solubilized proteins were reacted with Protein-G Sepharose (Amersham Biosciences) cross-linking with mAb-N. The resin was extensively washed with a buffer containing 0.1% NP-40, 0.25 M sucrose, 2 mM melcaptoethanol, 0.3 M NaCl, 50 mM Tris-HCl or 10 mM Hepes (pH 7.4) and protease inhibitors, and then MG23 was recovered by overnight incubation with 0.1 mM mAb7 epitope peptide. After the elution, the epitope peptide was separated from MG23 by gel filtration (Sephadex G-50, GE healthcare). The purified native preparations were used for chemical crosslinking, EM imaging and channel recording.

Purification of recombinant MG23. A His-tag sequence (6xHis) was inserted into the rabbit MG23 cDNA at the site immediately downstream of the signal sequence between residues 34 and 35. The His-tagged MG23 cDNA was subcloned into the pPICZ vector and transfected into *Pichia pastoris* X-33 cells, and transformed yeast clones were cultured according to the instruction manual

(Invitrogen). During shaking culture the expression of recombinant MG23 was induced by 0.5% methanol for ~24 hrs at 30 ^{o}C, and yeast cells were harvested for preparing microsomal vesicles (*9*). Recombinant MG23 was solubilized in a buffer containing 1% NP-40, 0.25 M sucrose, 2 mM melcaptoethanol, 0.3 M NaCl, 50 mM NaPi (pH 7.4) and protease inhibitors at ~2 mg/ml protein for 45 min. After diluting the detergent content to 0.5%, insoluble materials were removed by ultracentrifugation and solubilized proteins were applied to Ni-Sepharose (GE healthcare). The resin was extensively washed, and recombinant MG23 was eluted with a buffer containing 0.1% NP-40, 0.25 M sucrose, 50 mM NaPi (pH 7.4), 0.3 M NaCl, 400 mM imidazole, 2 mM melcaptoethanol and proteinase inhibitors. The eluted solution was 3-fold diluted to reduce the imidazole concentration and applied to Protein G Sepharose cross-linking with mAb-C. After washing the resin with a buffer containing 0.1% NP-40, 0.25 M sucrose, 50 mM NaPi (pH 7.4), 0.3 M NaCl, 2 mM melcaptoethanol and proteinase inhibitors, recombinant MG23 was recovered by overnight incubation with 0.1 mM epitope peptide. After the elution, the epitope peptide was separated from MG23 by gel filtration. Using DDM instead of NP-40, recombinant MG23 was also solubilized and purified under essentially the same conditions. Recombinant MG23 was purified with either NP-40 for chemical crosslinking and EM imaging, or with DDM for channel recording experiments.

EM analysis. After affinity purification, MG23 were further separated by density gradient centrifugation. The 5-20% sucrose liner gradient containing the final elution buffer without the peptides was prepared and centrifuged for ~10 hrs in a Beckman SW41 rotor at 220,000xg. MG23-enriched fractions were detected by Western blotting, and used for EM analysis. For immuno-decoration of MG23 particles, mAbs were reacted with the purified preparations. MG23 particles with or without the immuno-decoration were applied to thin carbon films, negatively stained with 2% uranyl acetate solution, and analyzed using EM (JEM-100CX, JEOL) at 39,024x magnification with a 100-kV acceleration voltage. Images were recorded on SO-163 films (Eastman Kodak) and digitized with a Scitex Leafscan 45 scanner (Leaf systems) at a pixel size of 0.256 nm at the specimen level.

Particle image analysis. Particle 3D reconstruction was performed essentially as described in previous works (*7, 16*). MG23 projections were primarily selected in 160 x 160 pixel subframes (corresponding to 41 x 41 nm) using the auto-accumulation method with simulated annealing (*18*). Selected particles were rotated at 10^{o} increments to generate a set of training images for the three-layer pyramidal-type neural network (*17*). The trained neural network selected additional particles for a total of 23,173 particle images. Because of limited resolution, contrast transfer function correction was not performed for the particle images in this analysis. In highly-purified MG23 preparations, predominant particles were about 17-19 nm in length and 14-16 nm in width,

and appeared to have 6-fold symmetry. The minor particles had a smaller size (about 13-17 nm in length and 6-8 nm in width) and asymmetrical structures, which appeared to be a component of the predominant particle. For reconstruction, we used 11,175 images for the large-sized group and 1,707 for the small-sized group. Each particle image library was processed separately in the following steps. Particles in each library were aligned rotationally and translationally (*19-21*) relative to each other using the reference free method (*17*). Aligned images were classified into 250 clusters for the larger-sized group and 120 for the smaller-sized group using the Modified Growing Neural Gas Network method (*22*) and Multivariate Statistical Analysis (*23*), respectively. The resulting class averages were used as new references and the cycle from alignment to classification was repeated until convergence. After convergence, the class averages were examined to test the presumption of symmetry. For the larger-sized group, we obtained averaged particle images showing highly symmetrical futures, and 6-fold symmetry was imposed in the following computation based on the putative top view image (Figure 4A, second row). Since the smaller-sized group did not show any apparent symmetry, no symmetry was assumed for the calculation. An Euler angle was assigned to each average image, using the Echo-Correlated 3D Reconstruction Algorithm (*24*). The first 3D model was reconstructed using the SIRT method (*25*) from averages with assigned Euler angles and used as the reference model for the next step. To optimize 3D reconstruction using projection matching (*26*), reprojection images were created from the 3D model. Using these as references, the particles in the library were rotationally and translationally aligned by the Multi-Reference Alignment method. The aligned particles were further classified using the same classification algorithm as above. For each average image, an Euler angle of the reprojection image was assigned so as to show the best correlation to the average. These steps were repeated until the 3D model was stabilized. During these iterations, the Echo-Correlation method was used to optimize the Euler angles of class average images.

SUPPLEMENTARY FIGURES

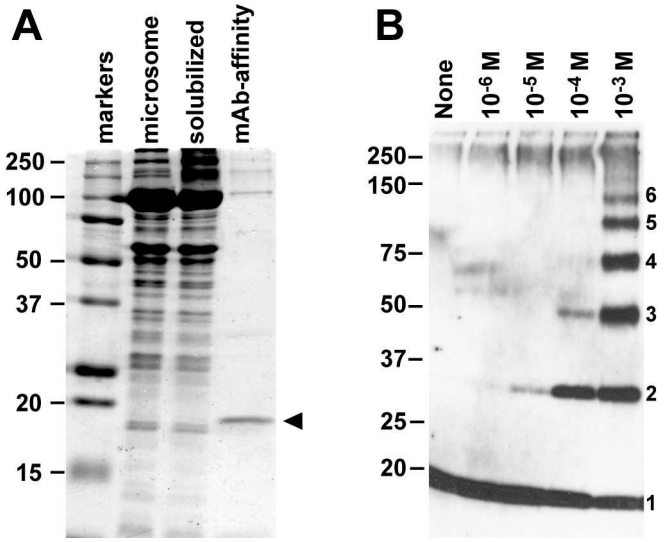

Figure S1: Purification and crosslinking of rabbit skeletal muscle MG23. (A) Purification of native MG23 purified from skeletal muscle. Aliquots of total microsome, solubilized microsomal fraction and immunoaffinity-purified fraction were analyzed on an SDS-PAGE. Proteins were visualized by Coomassie-blue staining. Native MG23 is marked by an arrowhead. (B) Chemical crosslinking of native MG23 purified from skeletal muscle. An affinity-purified native MG23 preparation was treated with the crosslinker disuccinimidyl glutarate at 10^{-6}~10^{-3} M, and resulting products were examined by immunoblotting using mAb-N; monomeric to hexameric products are numbered. Size markers are indicated in kDa.

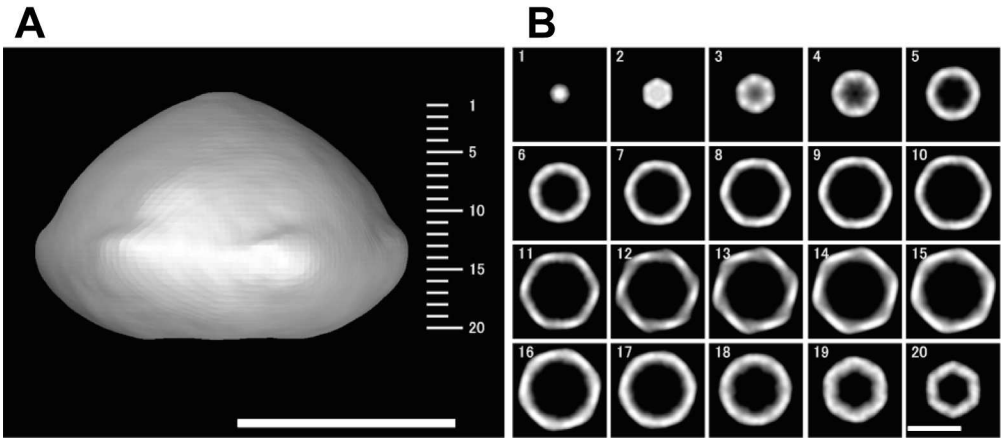

Figure S2: Structural features of MG23. (A) Surface representation of MG23 viewed from the side. Protein is displayed in bright shades. (B) Horizontal sections parallel to the membrane plane. The sections were prepared at 5.4 Å intervals and are numbered in the panel A (1 to 20). The data confirm that MG23 full-particle is a bowl-shaped molecule. The density at the central top is slightly lower than that of the surrounding part. The thickness of the lateral wall is estimated to be 28-35 Å and is larger than the typical diameter of a single α-helix. Therefore, the lateral wall might be composed of a couple of transmembrane segments. It is also possible that lipid and detergent components attached with the purified particles are involved in the reconstructed 3D volume, since both detergents and lipids are easy to adhere to hydrophobic regions, especially to membrane-spanning segments in integral membrane proteins. Scale bar represents 100 Å.

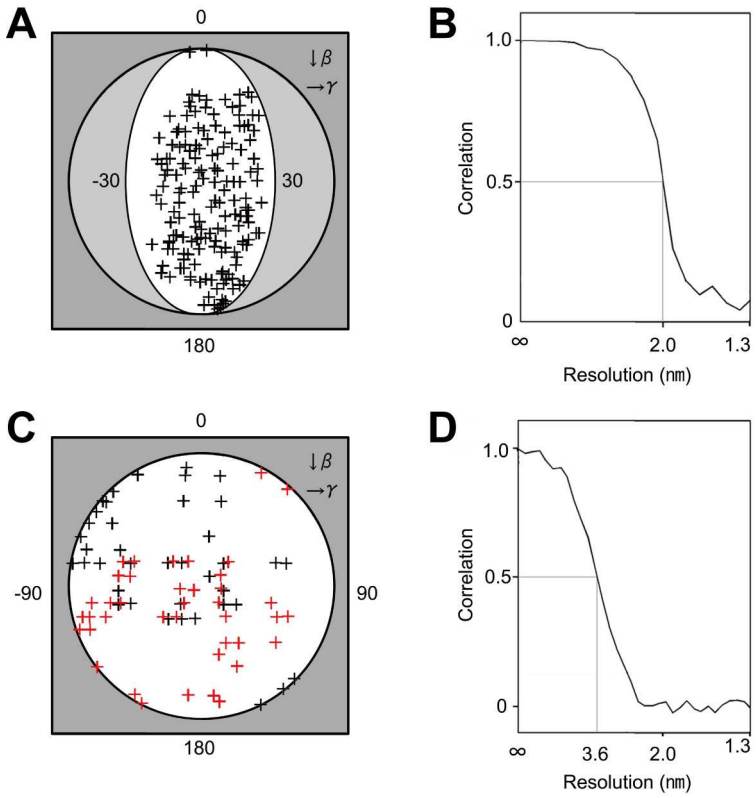

Figure S3: Euler angle distribution and FSC function of the MG23 reconstructions. (A and B) Reconstruction of the large bowl-shaped particle. (A) Surface projection of Euler angles of the 163 adopted class averages shows that the larger particles are almost randomly oriented on the grid surface. (B) According to the FSC function, the resolution limit of the large MG23 particle is 2.0 nm by the correlation coefficient 0.5 criterion. (C and D) Reconstruction of the smaller crescent-shape particles. (C) Surface projection of Euler angles of the 117 adopted class averages. Red crosses indicates their positions are on the far side of the globe. (D) The resolution limit of the small MG23 particle was shown to be 3.6 nm by the correlation coefficient 0.5 criterion.

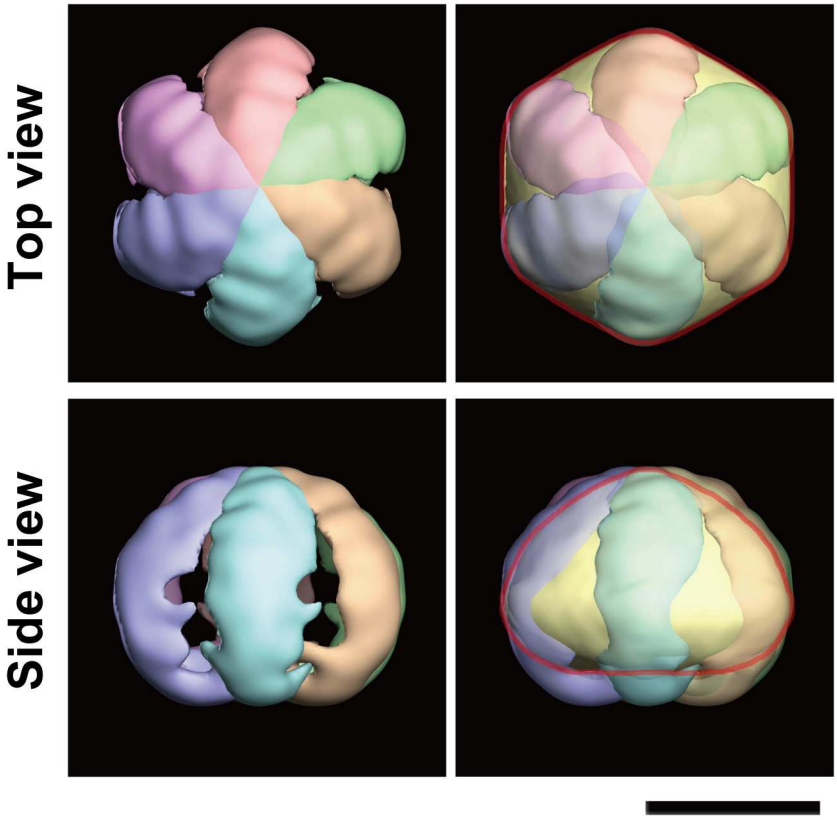

Figure S4: Proposed configuration of the six-subunit assembly. In this model, the large bowl-shaped structure (full-MG23 particle) was fitted with the six crescent-shaped subunits (putative hexameric subunit). This configuration assumes that each subunit is located longitudinally at 60-degree intervals (left panels). Volume of the full-MG23 was contoured at 828 kDa (yellow mass with red outline) assuming a hexagonal assembly of the 138-kDa (23 kDa x 6) hexameric subunit, and superimposed to the subunit assembly (right panels). The outline from the top resembles each other, but in the side view, the crescent-shaped subunits are slightly long and narrow to fill to the full-MG23. The discrepancy in fitting may suggest the conformational changes of each subunit during assembling into full-MG23 particles. Scale bar, 10 nm.

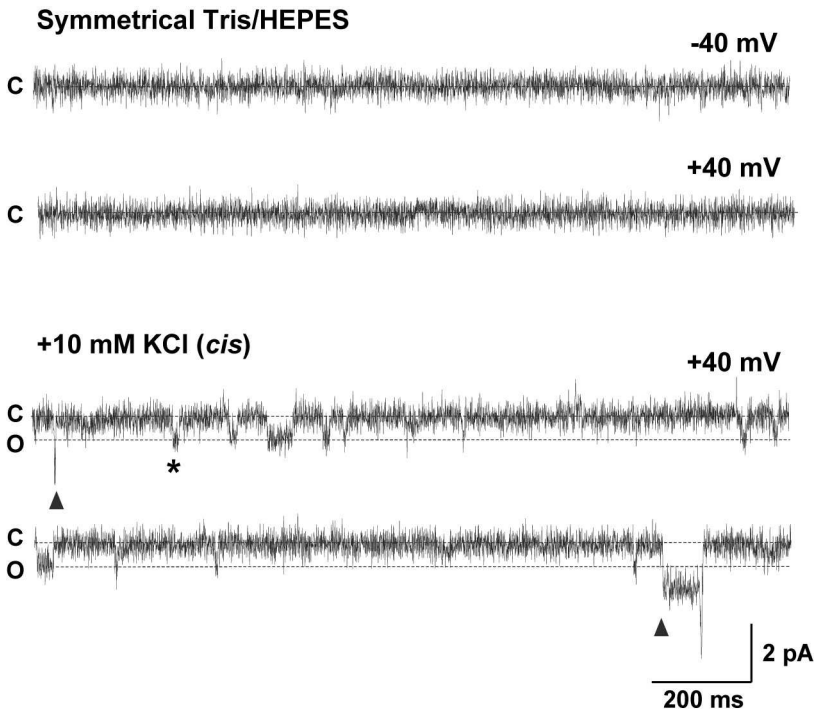

Figure S5: MG23 does not conduct Tris or HEPES. Liposomes containing recombinant MG23 were fused with a bilayer in a solutions containing KCl so that fusion events could be monitored. Immediately following fusion, the *cis* and *trans* chambers were perfused with solutions containing 250 mM Tris/HEPES, pH 7.2. No single-channel events were observed under these recording conditions either at -40 mV (top trace) or +40 mV (second trace). After addition of 10 mM KCl to the *cis* chamber, single MG23 opening events (the asterisk shows an example) and co-ordinated openings of multiple MG23 channels (arrows) could be observed due to K^+ flux in the *cis* to *trans* direction. C and O indicate the zero current level (all channels closed) and the current level of a single MG23 channel opening, respectively.

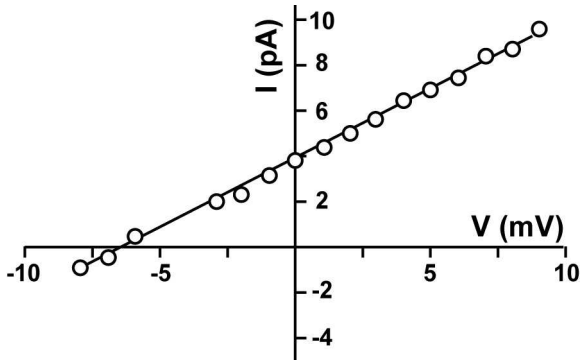

Figure S6: MG23 current-voltage relationship under bi-ionic conditions. An example of an MG23 current-voltage relationship obtained with 210 mM K^+ in the *cis* chamber and 65 mM Ca^{2+} in the *trans* chamber is shown. All experiments were performed with bilayers that contained multiple MG23 channels. This was necessary partly because the single-channel conductance of MG23 is small, partly because it is rare to obtain bilayers where only a single-channel has incorporated and partly because the low open probability of MG23 at voltages higher than -20 mV makes it difficult to measure openings close to the reversal potential. The figure shows a single example of an experiment rather than showing the average data. This is because each bilayer experiment contained such a variable number of active MG23 channels that the mean currents at each voltage are vastly different. We therefore plotted each bilayer experiment individually and calculated the reversal potential for each experiment. The figure shows predominantly positive holding potentials because as the potentials become more negative, this induces the opening of many more channels leading to an average current that is huge and variable (see Figure 7C). The current-voltage relationship has been corrected for the liquid junction potential that arises between the two different solutions and yields a reversal potential of -6.35 mV. The mean reversal potential from 3 similar experiments was -6.9 ± -3.7 mV (SD; n = 3).